Pramana–J. Phys. (2024) **123**: ####
DOI 12.3456/s78910-011-012-3

Crystallization of Liquid Silica under Compression: A Molecular Dynamics Simulation

NGUYEN VAN HONG [1*], NGUYEN HOANG ANH [2]

[1] Hanoi university of science and technology, Hanoi, 100000, Vietnam
[2] Colorado School of Mines, Golden, Colorado, 80401, USA

[*]Corresponding author. E-mail: hong.nguyenvan@hust.edu.vn

MS received 17 May 2024; revised 29 July 2024; accepted 02 August 2024

Abstract. In this study, we employ molecular dynamics simulations to develop a large model (19,998 atoms) of liquid SiO_2 at 3500 K. We construct models at different pressures in the 0-100 GPa range using the BKS potential and periodic boundary conditions. The goal is to detail the structural transition from the polyamorphic liquid state of SiO_2 to the crystalline stishovite form, which occurs between 45 and 60 GPa. We analyze the polyamorphic state of liquid SiO_2 by examining the formation of SiOx clusters from 2 GPa to 60 GPa. Beyond 60 GPa, the Pair Radial Distribution Functions (PRDFs) for Si-O, O-O, and Si-Si display multiple peaks, indicating the crystalline phase. This observation is further supported by examining the bond angle distribution, the fraction of SiOx units and OSix linkages, Si-O bond lengths within SiOx units, structural visualizations, and the analysis of ring statistics in the liquid SiO_2 system, all of which underscore the comprehensive changes in the system's structure.

Keywords. liquid SiO_2, stishovite, SiO_2, ring statistics, polyamorphism, crystallization.

PACS Nos 61.30 ; 61.10; 61.43.Fs

1. Introduction

In recent decades, glass and liquid silica (SiO_2) have garnered significant attention from researchers due to its diverse applications in engineering materials and its relevance in earth sciences [1–7]. Grasping the densification mechanisms within this material is essential for addressing questions related to the process of crystallization, the development of ceramics with enhanced toughness, and composition of the Earth's upper and lower mantle boundary [8,9]. Molecular dynamics simulations (MDS) are used to explore the equilibrium interface between the high-density liquid (HDL) and low-density liquid (LDL) phases of silica [10]. The investigation reveals a transition from fragile to strong dynamics across the silica HDL-LDL interface. Dynamic property analysis uncovers three distinct types of dynamical heterogeneity merging at this interface. Furthermore, crossing from the HDL to the LDL side leads to a significant increase in the Si/O coordination number ratio, marking a narrow zone where there's considerable mixing between the HDL and LDL phases. During compression, liquid SiO_2 simultaneously harbors both low-density and high-density phases. The scale of these phase region is notably affected by the degree of compression applied [11]. The polymorphic phenomenon of liquid systems under compression is not exclusive to silica; other compounds like beryllium fluoride (BeF_2) [12], germania (GeO_2) [12–14], alumina (Al_2O_3) [15], boron trioxide (B_2O_3) [16], the mixture of Yttrium Oxide and Aluminum Oxide (Y_2O_3-Al_2O_3) [17] also exhibit this behavior. Besides MDS, ab initio method is the useful tool that is extensively applied to analyze microstructural evolution during solidification and structural phase transformations [18-21]. Despite numerous investigations into the crystallization of glass SiO_2 and the polyamorphism of liquid SiO_2, the detailed mechanism underlying the structural phase transition from the polyamorphic state of liquid SiO_2 to crystalline stishovite SiO_2 have not been yet clarified. Especially, the ring statistics of liquid SiO_2 are still in question. This study aims to shed light on the complex transition. Furthermore, by employing molecular dynamics simulations, we have developed a liquid SiO_2 model comprising an expansive atomic ensemble of 19,998 atoms. This substantial increase in the number of atoms allows for a more refined and higher quality research model than those limited to only a few

thousand atoms, enhancing our ability to discern the intricacies of the structural phase transitions in SiO_2.

2. Methodology

In this work, the MDS is conducted on a model consisting of 19,998 atoms, including 6,666 Si and 13,332 O particles, utilizing the Beest–Kramer–Santen (BKS) potential and periodic boundary condition. This potential is extensively applied in the examination of silica in both its liquid and glass states [22–25]. Details regarding the BKS potential utilized can be found in the work of B. van Beast et al. [26]. In this study, the Verlet algorithm is employed with a timestep of 0.48 fs. The process begins with a random distribution of particles within the simulation box, which is subsequently heated to 6000 K to eliminate the initial configuration (to assure the model does not depend on initial configuration). Following this, the system is sequentially cooled at a cooling rate of 2.5 K/ps to temperatures of 5000, 4500, 4000 K with relaxation at each temperature stage, and eventually 3500 K. When reaching the final temperature of 3500 K, the system undergoes an extended relaxation phase for 107 MD timesteps within the NPT ensemble, resulting in the formation of the liquid SiO_2 model in equilibrium state at ambient pressure (0 GPa). The model is then subjected to compression to achieve the desired pressures from 0 to 100 GPa. The analysis for each model is conducted by averaging the data collected from the last 1000 MD steps. For structural analysis, calculations are made for Si-O, O-O, and Si-Si bond length distributions, Si-O-Si and O-Si-O bond angle distributions, the proportions of SiOx units and OSix linkages, SiOx cluster formation, formation of edge- and face-sharing linkages, and the statistics of ring structures under varying pressures.

3. Results and discussion

3.1 *The bond length of Si-O, O-O and Si-Si under compression*

In order to understand the structural phase transition during the compression process, this study focuses on the local structure of the -Si-O- network, the Short-Range Order (SRO), and the Intermediate-Range Order (IRO) under conditions of compression. Figure 1 illustrates the variations in the PRDFs of Si-O, O-O, and Si-Si as pressure is applied. The IRO is analyzed based on formula $2\pi/Q$ where Q represents the position of the first sharp diffraction peak [27]. At ambient pressure, the first peaks of the Si-O, O-O, and Si-Si PRDFs are found at 1.60, 2.63, and 3.11 Å respectively, aligning well with findings from prior research [22,28–30]. As pressure escalates, the first peak of the Si-O PRDF remains relatively stable in position, yet its height diminishes and the full width at half maximum (FWHM) expands, indicating a reduction in SRO.

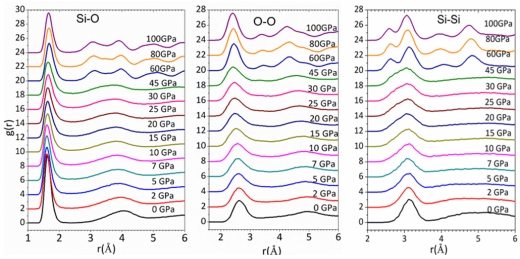

Figure 1. Figure 1. PRDF of Si-O, O-O and Si-Si at different pressures.

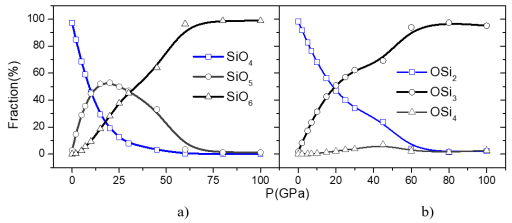

Figure 2. The fraction of SiOx (x = 4, 5, 6) units (a) and OSix (x = 2, 3, 4) linkages (b) at different pressures.

Above 60 GPa, the presence of multiple peaks in the PRDFs for Si-O, O-O, and Si-Si suggests a phase transition from the polyamorphic state [15] of initial liquid SiO_2 to a crystalline phase. As pressure increases, the first peak in the O-O PRDF shifts to the left continuously, while the first peak in the Si-Si PRDF splits into two distinct sub-peaks starting at 60 GPa. This division in the Si-Si PRDF can be attributed to the emergence of edge-sharing and face-sharing bonds under high pressure (see Appendix - Table 1), alongside changes in the Si-O-Si angle distribution caused by the formation of OSi_3 units. Given that both liquid and glassSiO_2 exhibit a random, continuous network characteristic of polyamorphism, the transition from liquid SiO_2 to glassSiO_2 with increasing pressure is not clearly delineated by changes in the PRDFs for Si-O, Si-Si, and O-O. However, during crystallization, the IRO of the crystal network markedly diverges from the continuous random network, enabling the identification of the crystallization phase between 45 and 60 GPa in liquid SiO_2. The emergence of numerous peaks in the PRDFs of SiO_2 also aids in elucidating the crystallization process of glassSiO_2, though for glassSiO_2, crystallization occurs under significantly lower pressures which is below 35 GPa [31–34].

Figure 2 presents a comprehensive analysis of the

pressure-dependent variations in the abundance of SiOx (x = 4, 5, 6) fundamental units and OSix (x = 2, 3, 4) linkages. At ambient conditions, the system predominantly comprisesSiO_4 tetrahedral units, which tend to form networks mainly via bridging oxygen atoms that are associated with OSi_2 linkages. Upon the application of pressure, a remarkable transition occurs within this network. TheSiO_4 units, initially the majority species, experience a substantial decline in their relative fraction while the fraction of SiO_5 andSiO_6 units increase. In the case of SiO_5, the fraction reaches the maximum value of about 50Insights into the structure of SiOx are also derived from analyzing bond angle distributions of O-Si-O and Si-O-Si. These angles illuminate the internal atomic arrangement and the inter-unit connectivity within SiOx, respectively. Bond angle distributions under compression forSiO_4,SiO_5, andSiO_6 units are detailed (see Figure 3). At ambient pressure, theSiO_4 units has the peak of 109°, it is near to the value of 107 ± 2° [22,26]. InSiO_2 glass, these are value are in range from 109.5 to 109.7° [35–39]. The revealing that the O-Si-O angle in idealSiO_4 tetrahedra to form an ideal tetrahedrally bonded random network. At higher pressure, the bond angle distribution slightly shifts to the left, indicating that the tetrahedra distort due to tension. ForSiO_5 andSiO_6, the angle distributions peak at around 90°, however, inSiO_6, there is another peak at around 167°, suggesting distinct structural characteristics. Under compression, the O-Si-O angle distribution of SiO_4 slightly shift to the left, reaching the value of around 105° at 30 GPa. The O-Si-O angle distribution of SiO_5 remains unchanged at different pressures. InSiO_6, two peaks are more pronounced from 60 GPa compared to their shapes at low pressures and the FWHM is narrower. Along with the PRDF distribution of Si-O, Si-Si and O-O (see Figure 1) and the system from 60 GPa consisting mostly of SiO_6.

In exploring the structural transition of liquid SiO_2 under varying pressures, particularly through the lens of Si-O-Si bond angles within OSix linkages (x = 2, 3, 4) as depicted in Figure 2.b, we observe a nuanced interplay between pressure, bond angle distribution, and structural transformation. At ambient pressure, the distribution of Si-O-Si in OSi_2 linkages manifest Si-O-Si bond angles around 145°, it is in good agreement with a previous work [22] . This configuration undergoes a small shift towards 140° at 30 GPa, hinting at the initial stages of structural rearrangement. Contrastingly, the Si-O-Si bond angle distributions for OSi_3 and OSi_4 linkages at similar pressures present a broader spectrum. The absence of a definitive peak in OSi_3 linkages suggests the transition towards more complex geometries that bridge tetrahedral and higher-coordinated structures. OSi_4 linkages, with a notable peak near

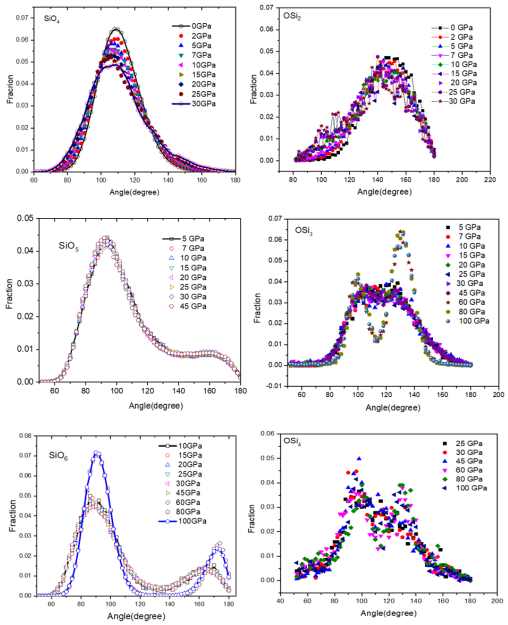

Figure 3. O-Si-O bond angle distributions in SiO_4, SiO_5 and SiO_6 units (left) and Si-O-Si bond angle distributions in OSi_2, OSi_3 and OSi_4.

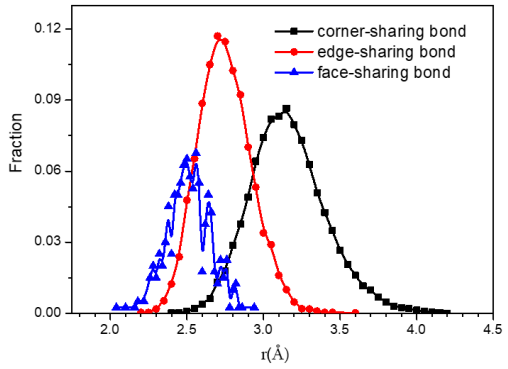

Figure 4. The average bond lengths of corner-, edge- and face-sharing bonds at 100 GPa.

100°, signal significant emergence of six-fold coordinatedSiO_6. The transition observed at pressures exceeding 60 GPa, marked by the shift from a singular to dual peak distribution in Si-O-Si bond angles at 100° and 131° for OSi_3 and OSi_4 linkages, underscores a significant reconfiguration of theSiO_2 molecular network. The reduction in the Si-O-Si bond angles contributes to shorter Si-Si bond lengths, which in turn increases Coulomb repulsion force [26] between the two Si atoms [34]. This escalation in repulsive forces leads to an elongation of Si-O bond lengths. Consequently, the Si-O-Si bond angle distribution's dual peaks in OSi_3 and OSi_4 lead to the splitting of the Si-Si PRDF first peak into two different subpeaks, measured (see Figure 1), respectively.

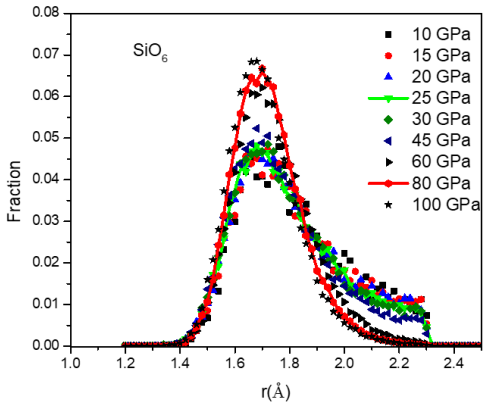

Figure 5. The Si-O distance distribution inSiO_6.

At ambient pressure, the liquid SiO_2 is composed of SiO_4 units what connect to others by corner-sharing bonds. When the pressure increases, the edge-sharing and face-sharing bonds appear (see Appendix - Table 1) and contribute to forming the -Si-O- network and the relative fractions of those bonds also depend on pressure. At pressures exceeding 60 GPa, the first peak of the Si-Si PRDF split into two distinct subpeaks, located at 2.59 Å and 3.05 Å, as depicted in Figure 1. This phenomenon is attributed to the emergence of edge- and face-sharing bonds under high pressure conditions. The interplay between the average bond lengths of edge- and face-sharing linkages and the splitting of the first peak is corroborated by many works, ranging fromSiO_2 [40] to GeO2 [41] and other variousSiO_2-based materials [42–44]. Figure 4 illustrates the bond length distribution across the three types of bonds. At a pressure of 100 GPa, the mean bond lengths for corner-sharing, edge-sharing, and face-sharing bonds are determined to be 3.12 Å, 2.72 Å, and 2.53 Å, respectively. These measurements reveal a direct correlation between bond lengths and the splitting of the Si-Si PRDF first peak in high pressure environments. In particular, the lengths of edge- and face-sharing bonds correspond to the first subpeak, whereas the length of corner-sharing bonds aligns with the second subpeak. The slight deviation of the second subpeak from the peak position associated with corner-sharing bond lengths is attributed to the superposition of bond length distributions among these three bond types.

Stishovite, a highly scrutinized phase of silica, features a distinctiveSiO_6 octahedral structure, setting it apart from other silica polymorphs with its denser silicon and oxygen atom arrangement [32]. This tetragonal structure is notable for its six-coordination of Si atoms [34], a contrast to the four-coordination observed in quartz and similar silica forms, presenting a more compact formation. In liquid SiO_2, the proportion of SiO_6 units significantly increases as pressure rises (see Figure 2). The distribution of Si-O distances withinSiO_6, shown in Figure 5, centers around 1.69 Å. It is observed that with increasing pressure, the peak of the Si-O distance distribution becomes more pronounced. The Si-O bond lengths withinSiO_6 at pressure in a range from 60 GPa to 100 GPa are more stable compared to those at lower pressures, contributing to the formation of a more orderly stishovite crystal structure. The emergence of SiO_6 units plays a crucial role in the crystallization of SiO_2 under compression, as evidenced in studies [45,46]. In previous research, aSiO_2 glass sample is compressed across a range from 0 to 100 GPa [47]. The coordination number of Si in the glass transitions from 4 to 6 at pressures between 20 and 35 GPa, maintaining this six-fold coordination up to 100 GPa. This change aligns with observations of six-coordinatedSiO_2 under compression, suggesting that the stishovite crystallization phase initiates at 35 GPa [48]. Notably, the Si-O distance inSiO_2 glass at this pressure is approximately 1.71±0.2 Å, closely matching the Si-O distance inSiO_6 units at 60 GPa of liquid SiO_2 observed in this study. The Si-O distances inSiO_6 units of liquid SiO_2 at the phase transition pressure are longer than those in glassSiO_2 due to the higher pressure applied. Based on these observations, we propose that the initial liquid SiO_2 system undergoes a transformation into a polymorphic state and subsequently transitions into a stishovite structure at 60 GPa. Figure 6 shows the partial snapshot of theSiO_2 system under compression. In the range from 0 to 45 GPa, the structure of the system appears disordered. However, a significant transformation is observed as the pressure increases from 60 GPa to 100 GPa, where the system exhibits a marked increase in orderliness. This transition underscores the progression towards crystalline formation, serving as a compelling piece of evidence that supports the emergence of a more structured and organized phase within theSiO_2 system under high-pressure conditions. This sequence of changes effectively illustrates the dramatic shift from a disordered to an ordered state, reinforcing the understanding of how pressure influences the structural dynamics and crystallization process of SiO_2.

The distribution of SiOx cluster sizes plays a pivotal role in the investigation of polymorphism within a given system [49,50]. Table 1 illustrates how the SiOx cluster sizes vary across pressures ranging from 2 to 60 GPa. At a pressure of 2 GPa, the majority of SiO_4 units are interconnected, forming a large cluster comprising 18,447 atoms, alongside 4 isolatedSiO_4 units (5 atoms each). TheSiO_5 clusters are relatively smaller, with a maximum size of 100 atoms. There are 21 isolatedSiO_6 units present at 2 GPa. With an increase in pressure, the largeSiO_4 clusters fragment into smaller parts, which

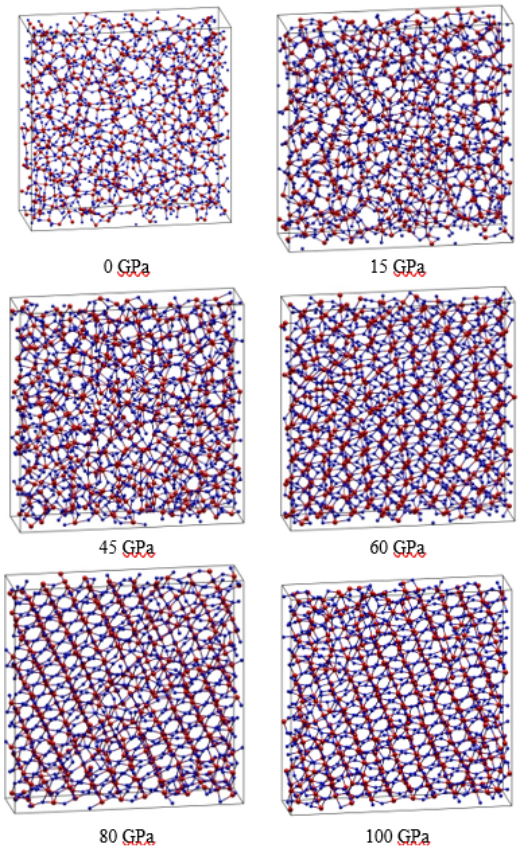

Figure 6. The -Si-O- network change under compression.

leads to the formation of largerSiO_5 andSiO_6 clusters. The largestSiO_4 cluster diminishes significantly in size with increasing pressure, from 16,064 atoms at 5 GPa to just 30 atoms at 30 GPa. By 60 GPa,SiO_4 clusters are absent, leaving behind 14 isolatedSiO_4 units. ForSiO_5 clusters, the size peaks at 14,398 atoms at 15 GPa, which is indicative of the highest relative fraction of SiO_5 in the system, as depicted in Figure 2, before sharply declining to 50 atoms at 60 GPa. The maximum size of SiO_6 clusters shows a small increase at pressures up to 15 GPa. At 30 GPa, the largestSiO_5 cluster consists of 13,319 atoms. The pronounced change in the sizes of SiO_4,SiO_5, andSiO_6 units under varying pressures from 2 to 60 GPa and the nonuniform spatial distribution of them contribute to the system's polymorphism. Intriguingly, at 60 GPa, all theSiO_6 units are interconnected to form a single cluster, which supports the notion that the crystallization process concludes at this pressure.

3.2 *Phase transition determined by density*

The structure of liquid SiO_2 is comprised of two distinct states, or phases: a low-density phase and a high-density phase [51–53]. The low-density phase features a network structure primarily formed through OSi_2 linkages and the high-density phase's network structure is built around OSi_3 linkages. As pressure increases, there is a notable increase in OSi_3 linkages, leading to more edge-shared links within the structure. This pressure-induced increase in edge-sharing linkages causes changes in the intermediate-range order (IRO) of the liquid SiO_2's network structure. In the regime of applied compressive forces,SiO_2 exhibits a continuous phase transition from a lower-density configuration predominated by OSi_2 linkages to a higher-density configuration predominated by OSi_3 linkages [15,54]. In the system, OSi_4 linkages account for a small percentage (see Figure 2). Therefore, to simplify the calculation, we ignore the existence of OSi_4 linkages. Figure 7 shows the varying density of the model with pressures. The density of SiO_2 is about 2.4 g/cm3 at 0 GPa and around 4.9 g/cm3 at 100 GPa. In the previous work [55,56], for the meltSiO_2 at the temperature range from 1900 to 2200 g/cm^3, the density of SiO_2, $\rho = 2.508 - 2.13 \times 10^{-4}T$ (g/cm^3), in which T is measured by Celsius. The structural constitution of liquid SiO_2 is an admixture of both low and high-density motifs within the interval. The density-specific structural networks are characterized by the predominance of either OSi_2 and OSi_3 linkages, with OSi_2 being indicative of the low-density phase and OSi_3 of the high-density phase. The density (ρ) of the SiO_2 system at a given pressure is quantifiable via the ratio of O–Si–O and O–Si–O_3 linkages as delineated in the following relation:

$$\rho_{\text{system}} = C_2\rho_L + C_3\rho_H \quad (1)$$

wherein C_2 and C_3 represent the fractional presence of O–Si–O and O–Si–O_3 linkages respectively, and ρ_L and ρ_H correspond to the densities intrinsic to the low and high-density states [15]. The density of the system depends on not only the respective fraction of O–Si–O, O–Si–O_3 but also the arrangement of SiO_x ($x = 4, 5, 6$) basic units in the network [**?**]. The fit of the simulation data to Eq. (1) is accurate, effectively capturing the phase transition of the system. The density of SiO_2 at 60 GPa is approximately 4.6 g/cm^3 in the simulation, closely aligned with a value of 4.7 g/cm^3 from the fitting data. These densities are approaching the 4.9 g/cm^3 observed at 100 GPa, indicating the completion of the phase transition from polyamorphic state to crystalline at around 60 GPa.

3.3 *Ring statistic of -Si-O- network*

To have a better understanding of structural transformation of -Si-O- network, we also analyzed the ring statistics of the system under compression. The network is conceptualized as an undirected graph, with each atom representing a node. This framework allows for a detailed examination of the network's connectiv-

Table 1. Distribution of SiOx-cluster size at different pressure. Ncl is the number of clusters; Nat is the number of atoms per one cluster.

2 GPa		5 GPa		10 GPa		15 GPa		30 GPa		60 GPa	
Distribution of SiO_4 cluster size											
Ncl	Nat	Ncl	Nat	Ncl	Nat	Ncl	Nat	Ncl	Nat	Ncl	Nat
4	5	34	5–10	282	5–10	486	5–10	391	5–10	14	5
1	18,447	2	11–20	35	11–20	93	11–20	18	11–20	-	-
-	-	1	16,064	15	21–30	42	21–30	5	21–30	-	-
-	-	-	-	1	33	11	31–40	-	-	-	-
-	-	-	-	1	41	11	41–50	-	-	-	-
-	-	-	-	1	52	23	51–100	-	-	-	-
-	-	-	-	1	168	5	101–300	-	-	-	-
-	-	-	-	1	9,537	-	-	-	-	-	-
Distribution of SiO_5 cluster size											
269	6–10	181	6–10	49	6–10	13	6	32	6–10	115	6–10
89	11–20	72	11–20	8	11–20	1	11	7	11–20	31	11–20
26	21–30	21	21–30	2	31–40	1	14,398	1	13,328	2	21–30
15	31–40	13	31–40	1	12,417	-	-	-	-	2	41–50
8	41–50	4	41–50	-	-	-	-	-	-	-	-
6	51–100	13	51–100	-	-	-	-	-	-	-	-
-	-	8	101–700	-	-	-	-	-	-	-	-
-	-	1	2,678	-	-	-	-	-	-	-	-
Distribution of SiO_6cluster size											
21	7	116	7	231	7	165	7	16	7	1	19,718
-	-	20	11–20	86	11–20	80	11–20	1	11	-	-
-	-	1	24	21	21–30	31	21–30	5	13,319	-	-
-	-	-	-	12	31–40	14	31–40	1	13,319	-	-
-	-	-	-	1	47	18	41–50	-	-	-	-
-	-	-	-	1	50	14	51–100	-	-	-	-
-	-	-	-	1	66	12	101–300	-	-	-	-

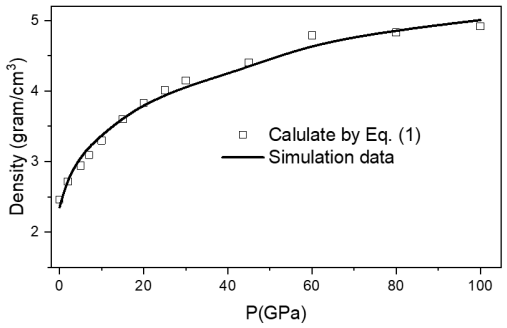

Figure 7. Density of SiO_2 of simulation data and based on Eq. (1).

ity, identifying paths as sequences of nodes and bonds connected in succession without overlaps [44]. The study of rings within such networks utilizes a variety of definitions [58–65], each offering a distinct perspective on the network's structure and properties. These methodologies differ in their approach to identifying and counting rings, which can lead to small variations in the calculated ring statistics. For this study, we employ the no shortcut path criterion and its associated algorithm as introduced by M. Matsumoto et al. [64]. This criterion is selected for its effectiveness in discerning ring structures within the -Si-O- network, defining an n-fold ring as a configuration consisting of n Si atoms and n O atoms. This methodological choice facilitates a targeted analysis of the network's ring structures, allowing for a deeper understanding of its geometric and physical characteristics. By adopting this approach, we contribute to a more comprehensive understanding of the network's structural intricacies. Figure 8 presents an in-depth analysis of the Si-O ring statistics in liquid SiO_2 under compression, focusing on rings up to a maximum size of 12, comprising 24 atoms (12 oxygen and 12 silicon atoms). At ambient pressure, the predominance of 6-fold rings is notably high. This observation is consistent with findings in vitreousSiO_2 systems [63-66]. The predominance of the 6-fold rings in both liquid and glass state can be attributed to the continuous random network structure formed by the fundamentalSiO_4 tetrahedral units that characterize both the glass and liquid states of SiO_2. The distribution of Si-O ring sizes exhibits a Gaussian shape at ambient pressure, which is closely tied to the

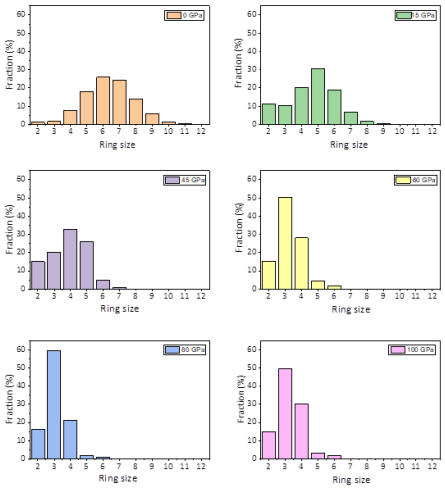

Figure 8. Si-O ring statistics under compression.

distribution of Si-O-Si and O-Si-O bond angles within the structure. These angles play a crucial role in the system's energy minimization, influencing the overall shape of the ring statistics. The formation of 2-fold rings (or edge-sharing bonds) and 3-fold rings occurs through shortening Si-Si distance, elongating of the Si-O bond and adjustments in the Si-O-Si and O-Si-O angles, aimed at reducing the system's energy. Consequently, these smaller rings represent only a minor fraction of the total. Larger rings, specifically those with 5, 6, and 7 members, display peak O-Si-O bond angle distributions approaching 109 degrees, indicative of nearly perfect tetrahedral configurations. Therefore, the 5, 6, 7-fold rings have the highest distribution in the system [66]. As pressure escalates, the large rings break down into small rings. There is a marked increase in the number of edge-sharing linkages (see Appendix - Table 1), leading to a significant rise in the prevalence of 2-fold rings between 0 and 15 GPa. Between 15 and 45 GPa, 5-fold rings become predominant, while 3-fold rings dominate the range from 60 to 100 GPa, accounting for 50-60

In the context of glassSiO_2, experimental data indicate a significant structural evolution with pressure, highlighted by the predicted and observed increases in the occurrence of 2-, 3-, and 4-fold rings [67, 68]. By Raman spectroscopy studies of glassySiO_2 under pressures ranging from 8 to 30 GPa [68], signifies a notable shift in the structural topology of the material. Comparatively, in crystalline stishovite [69], the dominance of 2-, 3-, and 4-fold rings mirrors the Si-O ring statistics observed in the high-pressure liquid SiO_2 system of this study. From this comprehensive analysis, we deduce a crystallization process occurring between 45 and 60 GPa, marking a transition from polyamorphism to the crystalline structure of stishovite in the initial liquid SiO_2 model, thus highlighting a critical pathway in the understanding of SiO_2's behavior under extreme conditions.

4. Conclusions

This study advances our understanding of the structural transformations and crystallization mechanisms in liquid SiO_2 under high-pressure conditions. By closely examining the local -Si-O- network structure and IRO through molecular dynamics simulations, significant insights have been obtained. The investigation reveals a complex transition from polyamorphic liquid SiO_2 to crystalline stishovite, highlighted by the evolution of Si-O, O-O, and Si-Si PRDFs under varying pressures. Notably, the structural transformation is most apparent in the pressure range of 5–60 GPa, where the system transitions through phases characterized bySiO_4,SiO_5, andSiO_6 units, eventually stabilizing in an octahedral network indicative of stishovite formation beyond 60 GPa. The analysis of bond lengths, bond angles, and coordination numbers under compression sheds light on the underlying mechanisms of silica's phase transition. The emergence of SiO_6 units and the corresponding changes in the Si-O-Si and O-Si-O bond angle distributions provide comprehensive evidence of silica's transition towards a more ordered and crystalline phase under high pressure. The ring statistics of SiO_2 under compression reveals a clear transition in the structural configuration of -Si-O- network, emphasizing the dominance of 6-fold rings at ambient pressure due to the continuous random network formed bySiO_4 tetrahedral units. Upon compression, a notable shift towards 5-fold rings up to 15 GPa, and subsequently 3-fold rings dominating at pressure from 60 to 100 GPa, indicates a significant structural phase transition. This shift is especially pronounced between 45 and 60 GPa, marking the transition from polyamorphism to a crystalline stishovite phase. The polyamorphic state of liquid SiO_2 is analyzed by the formation of SiOx clusters at pressure below 60 GPa. Experimental data further support this crystallization process, highlighting a crucial understanding of behavior of SiO_2 liquid under extreme pressure conditions. This insight into the pressure-driven structural phase transitions provides a deeper comprehension of the crystallization dynamics and the intricate behavior of liquid SiO_2. MDS and explorer discover analysis in this work can be applied to other glassy oxide systems such as germania and glassy silicate systems.

Appendix A.

Table-appendix: Distribution of the number of bonds per one Si4+ ion. Nc, Ne, Nf is the number of corner-edge and face-sharing bonds, respectively

Pressure (GPa)	Nc	Ne	Nf
0	2.01	0.02	0.00
2	2.13	0.08	0.00
5	2.28	0.19	0.01
7	2.40	0.26	0.01
10	2.50	0.37	0.02
15	2.68	0.54	0.03
20	2.86	0.63	0.05
25	2.96	0.73	0.04
30	3.03	0.82	0.06
45	3.21	1.00	0.08
60	3.83	1.04	0.02
80	3.93	1.02	0.01
100	3.87	1.07	0.02

References

[1] D. I. Grimley, A. C. Wright, and R. N. Sinclair, *J. Non. Cryst. Solids* **119**, 49 (1990).

[2] A. Takada, P. Richet, C. R. A. Catlow, and G. D. Price, *J. Non. Cryst. Solids* **345–346**, 224 (2004).

[3] C. Zhang and K. Najafi, *J. Micromechanics Microengineering* **14**, 769 (2004).

[4] A. Ashok and P. Pal, *Sci. World J.* **2014**, (2014).

[5] T. Tsuchiya and J. Tsuchiya, *Proc. Natl. Acad. Sci.* **108**, 1252 (2011).

[6] J. Sarnthein, A. Pasquarello, and R. Car, *Phys. Rev. B* **52**, 12690 (1995).

[7] A. N. Payzullaev *et al.*, *ECS Adv.* **2**, 031001 (2023).

[8] A. J. Gratz, L. D. DeLoach, T. M. Clough, and W. J. Nellis, *Science* **259**, 663 (1993).

[9] L. Huang, M. Durandurdu, and J. Kieffer, *Nat. Mater.* **5**, 977 (2006).

[10] X. Zhang *et al.*, *J. Chem. Phys.* **157**, 134703 (2022).

[11] L. T. San, N. V. Hong, and P. K. Hung, *High Press. Res.* **36**, 187 (2016).

[12] A. Takada, P. Richet, C. R. A. Catlow, and G. D. Price, *J. Non. Cryst. Solids* **353**, 1892 (2007).

[13] P. K. Hung and N. V. Hong, *Eur. Phys. J. B* **71**, 105 (2009).

[14] V. P. Prakapenka, G. Shen, L. S. Dubrovinsky, M. L. Rivers, and S. R. Sutton, *J. Phys. and Chem. of Solids*, Vol. **65** (2004), pp. 1537–1545.

[15] V. Van Hoang, *Phys. Lett. Sect. A Gen. At. Solid State Phys.* **335**, 439 (2005).

[16] L. Huang, J. Nicholas, J. Kieffer, and J. Bass, *J. Phys. Condens. Matter* **20**, 075107 (2008).

[17] P. F. McMillan *et al.*, *J. Phys. Condens. Matter* **19**, 415101 (2007).

[18] Gianfranco Sfuncia *et al.*, *CrystEngComm* **25**, 5810 (2023).

[19] Machado, M. A. *et al.*, *Cryst. Growth Des.* 24, 4717-4727 (2024).

[20] Zuo, M. *et al.*, *ACS Applied Engineering Materials* 1, 4, 1229-1240 (2024).

[21] Dai, Y., Song, M., *Materials Research* 22, 5 (2019).

[22] B. B. Karki, D. Bhattarai, and L. Stixrude, *Phys. Rev. B* **76**, 104205 (2007).

[23] B. B. Karki, D. Bhattarai, M. Mookherjee, and L. Stixrude, *Phys. Chem. Miner.* **37**, 103 (2010).

[24] A. Saksaengwijit and A. Heuer, *J. Phys. Condens. Matter* **19**, (2007).

[25] P. K. Hung, N. V. Hong, and L. T. Vinh, *J. Phys. Condens. Matter* **19**, 466103 (2007).

[26] B. W. H. van Beest, G. J. Kramer, and R. A. van Santen, "Phys. Rev. Lett. 64, 1955 (1990)."

[27] Y. Wang et al., "Nat. Commun. 5, 1 (2014)."

[28] Q. Mei, C. J. Benmore, and J. K. R. Weber, "Phys. Rev. Lett. 98, (2007).

[29] B. B. Karki, "Theor. Comput. Methods Miner. Phys. Geophys. Appl. 71, 355 (2018).

[30] Y. Waseda and J. M. Toguri, "Metall. Trans. B 8, 563 (1977)."

[31] D. Andrault, R. J. Angle, J. L. Mosenfelder, and T. Le Bihan, "Am. Mineral. 88, 301 (2003).

[32] K. J. Kingma, R. E. Cohen, R. J. Hemley, and H.-K. Mao, "Lett. to Nat. 374, 243 (1995).

[33] D. Andrault, G. Fiquet, F. Guyot, and M. Hanfland, "Science 282, 720 (1998).

[34] D. C. Palmer, R. J. Hemley, and C. T. Prewitt, "Phys. Chem. Miner. 21, 481 (1994).

[35] F. Mauri, A. Pasquarello, B. G. Pfrommer, Y. G. Yoon, and S. G. Louie, "Phys. Rev. B - Condens. Matter Mater. Phys. 62, R4786 (2000).

[36] M. R.L. and Warren B. E., "J. Appl. Crystallogr. 2, 164 (1969)."

[37] P. G. Coombs et al., "Philos. Mag. B Phys. Condens. Matter; Stat. Mech. Electron. Opt. Magn. Prop. 51, 39 (1985).

[38] J. Neuefeind and K. D. Liss, "Physical Chem. Chem. Phys. 100, 1341 (1996).

[39] R. F. Pettifer, R. Dupree, I. Farnan, and U. Sternberg, "J. Non. Cryst. Solids 106, 408 (1988).

[40] V. V. Le and G. T. Nguyen, "J. Non. Cryst. Solids 505, 225 (2019)."

[41] N. M. Anh, N. T. T. Trang, T. T. Nguyet, N. Van Linh, and N. Van Hong, "Comput. Mater. Sci. 177, 109597 (2020).

[42] N. H. Son, N. H. Anh, P. H. Kien, T. Iitaka, and N. Van Hong, "Model. Simul. Mater. Sci. Eng. 28, (2020).

[43] N. Hoang Anh, N. H. Son, and N. Van Hong, "VNU J. Sci. Math. - Phys. 39, 53 (2023).

[44] H. A. Nguyen and N. Van Hong, "Phys. Scr. 98, 0 (2023).

[45] T. Sato and N. Funamori, "Phys. Rev. Lett. 101, 255502 (2008).

[46] P. Dera, J. D. Lazarz, V. B. Prakapenka, M. Barkley, and R. T. Downs, "Phys. Chem. Miner. 38, 517 (2011).

[47] C. Meade, R. J. Hemley, and H. K. Mao, "Phys. Rev. Lett. 69, 1387 (1992).

[48] T. Sato and N. Funamori, "Phys. Rev. B - Condens. Matter Mater. Phys. 82, 1 (2010).

[49] M. T. Lan, T. T. Duong, N. V. Huy, and N. Van Hong, "Mater. Res. Express 4, (2017).

[50] L. T. San, N. Van Hong, T. Iitaka, and P. K. Hung, "Eur. Phys. J. B 89, (2016).

[51] T. Morishita, "Phys. Rev. Lett. 93, 055503 (2004)."

[52] D. Daisenberger et al., “Phys. Rev. B - Condens. Matter Mater. Phys. 75, 224118 (2007).
[53] E. Lascaris, M. Hemmati, S. V. Buldyrev, H. E. Stanley, and C. A. Angell, “J. Chem. Phys. 142, 104506 (2015).
[54] P. K. Hung, N. V. Hong, G. T. T. Trang, and T. Iitaka, “Mater. Res. Express 6, (2019).
[55] I. A. Aksay and J. A. Pask, “J. Am. Ceram. Soc. 62, 332 (1979).
[56] J. F. Bacon, A. A. Hasapis, and J. W. W. Jr., “Phys. Chem. Glas. 1, 90 (1960).
[57] P. Koziatek, J. L. Barrat, and D. Rodney, “J. Non. Cryst. Solids 414, 7 (2015).
[58] X. Yuan and A. N. Cormack, “Comput. Mater. Sci. 24, 343 (2002).”
[59] F. Wooten, “Acta Crystallogr. Sect. A Found. Crystallogr. 58, 346 (2002).
[60] D. S. Franzblau, “Phys. Rev. B 44, 4925 (1991).”
[61] K. Goetzke and H. J. Klein, “J. Non. Cryst. Solids 127, 215 (1991).”
[62] S. V. King, “Nature 213, 1112 (1967).”
[63] S. Le Roux and P. Jund, “Comput. Mater. Sci. 49, 70 (2010).”
[64] M. Matsumoto, A. Baba, and I. Ohmine, “J. Chem. Phys. 127, 134504 (2007).”
[65] T. Taniguchi, M. Okuno, and T. Matsumoto, “J. Non. Cryst. Solids 211, 56 (1997).”
[66] R. K. Kalia, A. Nakano, and P. Vashishta, “Phys. Rev. B 47, 3053 (1993).”
[67] K. Trachenko, M. T. Dove, V. V. Brazhkin, and J. C. Phillips, “J. Phys. Condens. Matter 15, (2003).
[68] R. J. Hemley, H. K. Mao, P. M. Bell, and B. O. Mysen, “Phys. Rev. Lett. 57, 747 (1986).
[69] C. J. Benmore et al., “Phys. Rev. B - Condens. Matter Mater. Phys. 81, 1 (2010).